Solution Processable Broadband Transparent Mixed Metal Oxide Nanofilm Optical Coatings via Substrate Diffusion Doping

Colm Glynn[a,b], Damien Aureau[c], Gillian Collins[a,d], Sally O'Hanlon[a], Arnaud Etcheberry[c], and Colm O'Dwyer[a,b]*

[a]*Department of Chemistry, University College Cork, Cork, T12 YN60, Ireland*

[b]*Micro-Nano Systems Centre, Tyndall National Institute, Lee Maltings, Cork, T12 R5CP, Ireland*

[c]*Centre de Spectroscopie, Institut Lavoisier de Versailles, Université de Versailles Saint Quentin-en-Yvelines, 78035 Versailles Cedex, France*

[d]*AMBER@CRANN, Trinity College Dublin, Dublin 2, D02 PN40, Ireland*

Devices composed of transparent materials, particularly those utilizing metal oxides, are of significant interest due to increased demand from industry for higher fidelity transparent thin film transistors, photovoltaics and a myriad of other optoelectronic devices and optics that require more cost-effective and simplified processing techniques for functional oxides and coatings. Here, we report a facile solution processed technique for the formation of a transparent thin film through an inter-diffusion process involving substrate dopant species at a range of low annealing temperatures compatible with processing conditions required by many state-of-the-art devices. The inter-diffusion process facilitates the movement of Si, Na and O species from the substrate into the as-deposited vanadium oxide thin film forming a composite fully transparent $V_{0.0352}O_{0.547}Si_{0.4078}Na_{0.01}$. Thin film X-ray diffraction and Raman scattering spectroscopy show the crystalline component of the structure to be α-$NaVO_3$ within a glassy matrix. This optical coating exhibits high broadband transparency, exceeding 90-97% absolute transmission across the UV-to-NIR spectral range, while having low roughness and free of surface defects and pinholes. The production of transparent films for advanced optoelectronic devices, optical coatings, and low- or high-k oxides is important for planar or complex shaped optics or surfaces. It provides opportunities for doping metal oxides to new ternary, quaternary or other mixed metal oxides on glass, encapsulants or other substrates that facilitate diffusional movement of dopant species.

*Correspondence and requests for materials should be addressed to Dr Colm O'Dwyer, Tel: +353 21 490 2732; Fax: +353 21 427 4097; Email: c.odwyer@ucc.ie

1 Introduction

Many modern applications and technologies are based on materials deposited upon transparent glass substrates.[1, 2] Devices formed on glass substrates are used in a wide range of applications such as electrochromics[3], thin film solar cells[4, 5], water splitting devices[6, 7] that could benefit from transparent electrodes,[8] optical coatings[9-11] and transparent thin film transistor (TTFT) technologies.[12-14] The type of coating deposited depends upon the transparent device application. Deposits can be used as electrical/active components or as buffer/dielectrics[15], both high- and low-k, between the substrate and active layers.[16] There are a variety of methods for depositing onto glass substrates, ranging from chemical/vapour depositions[17], sputtering[18] or solution processed[19] techniques. Each of these depositions typically entails a thin or thick film of the coating material being deposited onto the glass substrate and treated under a variety of processing conditions to attain the desired structure and morphology.[20-22] For optical coatings, the ability to conformally coat thin films on glass optics, non-planar surfaces that are index-matched to an application, or indeed as fully transparent invisible barrier or protection layers, are important for optics and photonics.

Transparent oxides (TO) see use in many modern technologies due to their novel metal oxide material characteristics coupled with high optical transparency over a range of wavelengths. TO materials can be used as a conductive channel in the case of transparent conducting oxides (TCO)[23, 24], as anti-reflection coatings[25] in optoelectronic devices and as active layers in thin film solar cells.[9, 19] Many of the transparent oxide materials, particularly TCO's, contain costly elements such as Indium or Gallium which in turn increases device costs; suitable replacement materials are crucial for some technologies, and atomic layer deposition (ALD) is a leading but expensive method for their production.[1] Device fabrication costs are also

linked to the complexity and number of processing steps during production. Therefore, since s-orbital states from the metallic species facilitate conduction in ionic mixed metal oxides of In, Ga, Zn and Sn for example, and not strongly influenced by structural defects and an amorphous state, considerable research is being conducted involving a replacement range of more abundant materials that are solution processable, particularly at processing temperatures <300 °C. Solution processed techniques are already a cost-effective deposition technique, where a liquid solution of the chosen material is prepared and deposited using a variety of methods such as spin-coating[22], dip-coating[26, 27] and inkjet printing[28, 29]. Using the solution processed techniques, the desired deposit can be formed through adjustments to the precursor solution and/or the deposition parameters[27, 30], and for optoelectronic devices, these routes offer low-temperature, solution-processable materials with excellent performance achievable with crystalline semiconductors, particularly in future applications where an electrically insulating optical material is required, such as in transparent TFTs featuring low-k materials.[31]

Many metal oxide materials have been extensively investigated in the search for new TCOs and in TTFT applications.[8] For each TO application a vast range of different materials and nanoscale assemblies exist. In TCO development, a variety of metal oxides can be used, most common of which being ITO,[8, 32, 33] however, porous arrangements of metal nanowire meshes[34] and composite materials utilizing graphene[35] with acceptable sheet resistances are under investigation. The nanoscale assembly, ranging from nanoparticles to nanowires, affects the optical and electrical characteristics of the material in both advantageous and disadvantageous ways. For example, an ITO thin film composed of epitaxial grown nanowires can exhibit high electrical conductivity and optical transparency while also benefiting from anti-reflective properties.[36] The benefit of TO materials in TFTs over Si based devices for TTFT technologies may require easier methods of deposition while retaining relatively high carrier and field effect

mobilities, and a defined optical transparency.[37] Advancements in TTFT technologies have benefited from the use of a variety of TO materials, in particular ZnO, IGZO and ZnSnO.[29, 38, 39] Through varied deposition conditions, thin films are produced with many different structures and compositions, ranging from amorphous to crystalline and importantly for many applications, using low temperature processing techniques.[40]

Many vanadium oxide (VO) materials see use in a variety of applications due to their optical and electrical properties depending upon the specific VO structure used, such as vanadium pentoxide (V_2O_5), dioxide (VO_2) and sesquioxide (V_2O_3).[41] The various VO materials are used as components in optoelectronic devices with applications in photovoltaics[4], metamaterials[42, 43], and electro/thermo-chromics.[3, 44] However, under normal deposition conditions the VO materials are not transparent by themselves in the visible spectral region. Controlling the diffusion process when doping metal oxides or forming ionic metal oxide mixtures with negligible surface irregularity remains a challenge. By utilizing a known thermally activated inter-diffusion effect experienced by some materials deposited on borosilicate glass, we show that a ternary mixed metal oxide V-O-Na-Si composite material is formed that is fully transparent from the UV to NIR spectral range at a processing temperature of 300 °C.

Here, we report how a uniform, continuous and smooth ternary mixed metal oxide transparent thin film (TTF) material is achieved from low temperature annealing of high-rate dip-coated VO based liquid precursors from inter-diffusion of substrate and precursor species in the film. The nature of the transparent mixed metal oxide thin film and formation process are examined using detailed Raman scattering, atomic force and electron microscopy, X-ray photoelectron and optical spectroscopy. Optical transparency, film structure and surface morphology of the TO material is demonstrated to depend upon the initial VO thin film thickness and both the temperature and duration of the thermal annealing step. Intermediate stages exist at

lower annealing temperatures where separate diffusion and crystallisation effects form multi-layered structures, each with unique optical and material characteristics. A low surface rms roughness of < 1 nm is retained for the TO thin films at each stage while the main absorption edge of the transparent material blue shifts to an E_g value of 3.7 eV, widening the broadband transmission window together with an increase in transmission to 90-97% across the UV to NIR spectral range, from reduced index and reflectivity. The surface composition of the thin films shows a predominantly O bonded Si glassy matrix, however, a complex structure is present due to the vanadia species dispersed within the material resulting in the formation of a $V_{0.0352}O_{0.547}Si_{0.4078}Na_{0.01}$ TTF material. The facile solution-processed technique that forms a transparent thin film material may be important for optical elements, optical coatings, photonic devices including LEDs, solar cells and those requiring low processing temperatures, and possibly as a low- and high-k film growth and invisible protective barrier layers.

2 Experimental

Preparation of VO precursor solution. Initial amorphous V_2O_5 thin films were deposited from an alkoxide based precursor solution. Vanadium (V) oxytriisopropoxide $[OV(OCH(CH_3)_2)_3]$ purchased from Sigma-Aldrich was mixed by volume with isopropyl alcohol (IPA) and deionized water at a ratio of 1000:10:1 (IPA : Alkoxide : H_2O) and stored with 4 Å molecular sieves from Sigma-Aldrich to prevent hydrolysis prior to deposition.

Substrate preparation and deposition of VO thin films. The thin films were deposited onto 1 mm thick borosilicate Thermo Scientific Microscope Slides. The composition of the glass slides is: SiO_2 72.20%, Na_2O 14.30%, CaO 6.40%, MgO 4.30%, Al_2O_3 1.20%, K_2O 1.20%, SO_3 0.30% and Fe_2O_3 0.03%. The glass substrates were cleaned prior to deposition using an acetone, IPA

and DI water procedure. A 30 minute UV-Ozone treatment was performed prior to dip-coating using a Novascan UV-Ozone system to remove any organics present on the surface. The initial V_2O_5 thin films were dip-coated using a PTL-MM01 desktop dip coater at a constant withdraw rate of 2.5 mm/s. Thermal treatments were performed at a variety of temperatures and times to form the TO films using a conventional oven in an ambient air atmosphere.

Thin film analysis techniques. Atomic force microscopy (AFM) was performed on a Park XE-100 AFM system in non-contact mode with SSS-NCHR enhanced resolution tips. The XY and Z resolutions of the AFM system are ~ 2 nm and ~ 0.05 nm respectively. Raman scattering spectroscopy was collected on a Renishaw InVia Raman spectrometer using a 514 nm 30 mW laser source. Spectra were collected using a RenCam CCD camera and the beam was focused onto the samples using either a 20× or 50× objective lens.

To measure the optical transparency of the samples in the 200 – 1000 nm range a Thermo Scientific Evolution 60S UV-Visible spectrophotometer illuminated with a Xenon light source with an accuracy of ±0.8 nm was used with a custom sample holder. To examine the optical transmission in the wavelength range of 1000 – 2500 nm an OceanOptics NIRQuest256-2.5 spectrometer was used with a 9.5 nm spectral resolution. An OceanOptics HL-2000 tungsten halogen source was used for illumination. Thin film X-Ray diffraction (XRD) was performed with a Philips X'pert equipped with a θ–θ goniometer. A Cu anode provided X-ray photons with a wavelength of λ = 0.15956 nm.

X-ray photoelectron spectra (XPS) spectra were collected on a Thermo Electron K-Alpha spectrometer using a monochromatic Al K_α X-ray source (1486.6 eV). Core level spectra from 100 scans were referenced to the C 1s core-level peak at 284.3 eV. The XPS spectra were

processed using a Shirley background correction followed by peak fitting to Voigt profiles. The FWHM were allowed to vary within reasonable value ranges in order to achieve best fit.

VO thin film and processing conditions. Each of the samples in this work was prepared with either 5 or 10 dip-coated layers of VO from the alkoxide based precursor. The samples under study are the untreated as-deposited (As-Dep) thin films and the same samples thermally annealed at low, intermediate and high temperatures (LTA, ITA, HTA), 200 ^{o}C, 250 ^{o}C and 300 ^{o}C respectively.

3 Results and Discussion

Figure 1 (a) shows the evolution of a 10 layer dip-coated VO thin film on glass to a completely transparent thin film (TTF) material formed after annealing. Optical images in Fig. 1 (a) show the initial dip-coated as deposited film and its intermediate stage formed through an intermediate thermal anneal (ITA) treatment, where the characteristic green-yellow colour changes to a dark yellow. Remarkably, the samples formed through a high thermal anneal (HTA) treatment at 300 ^{o}C show a complete transformation to a fully transparent coating, cleared entirely of its colour. The solution processed technique also allows for non-planar substrates to be used, such as the borosilicate glass tube shown in Fig. 1 (a). Both the inner and outer diameter of the tube can be conformally coated through dip-coating and the TTF subsequently formed through a HTA treatment.

The optical transmission from 300 – 2500 nm, including that of the underlying glass substrate, for the As-Dep, ITA and HTA treated thin films is shown in Fig. 1 (b) with a comparison of the transmission at select wavelengths presented in Fig. 1 (c). In Fig. 1 (b), a

distinctive change to almost complete visible transparency occurs due to the inter-diffusion between the substrate and the VO thin film. During the transition to optically cleared transparency (ITA samples annealed at 250 ^{o}C), the absolute transmission initially decreases below that of the as-deposited thin film across the broadband UV-NIR spectral range due to the crystallisation and densification of the thin film prior to its conversion to a full TO. This decrease in transmission is also observed in thin films of V_2O_5 deposited onto ITO coated glass substrates where the ITO acts as a diffusion barrier, and thus is related to crystallization and densification of the VO film (*vide infra*).[27, 45] However, the optical transmission markedly increases in the HTA thin film with a noticeable blue-shift in the absorption edge and increase in broadband transparency.

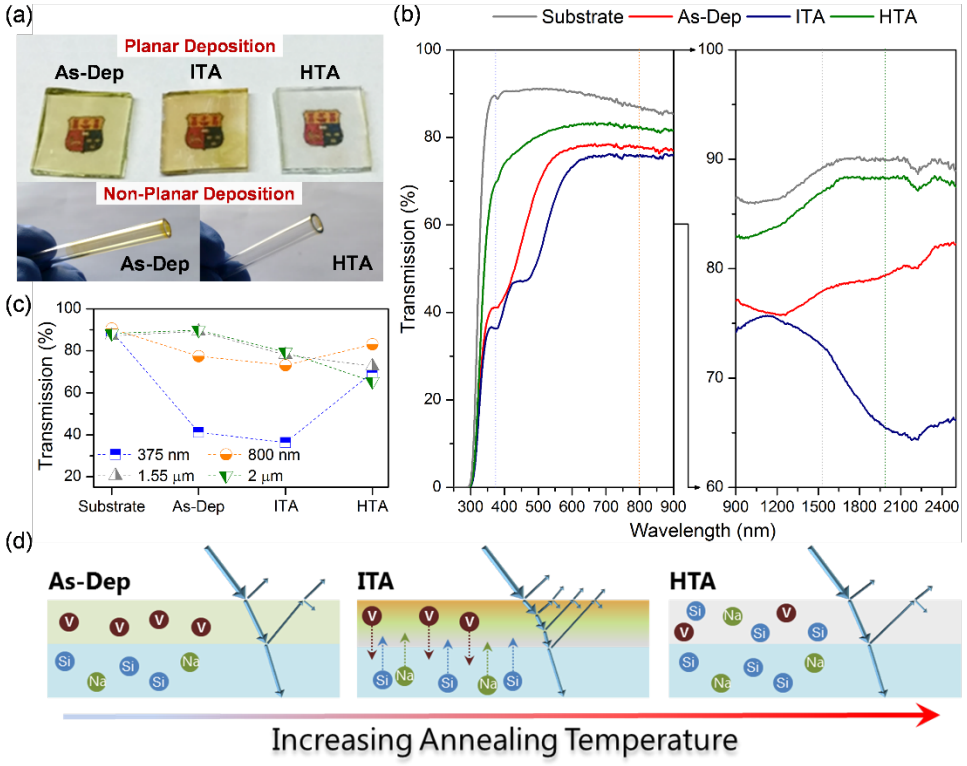

Figure 1. (a) Optical images of the As-Dep, ITA and HTA treated thin films on planar and non-planar glass substrates and (b) UV-Vis-NIR transmission spectra of the respective planar samples using air as the normalized background for 100% transmission (background spectrum shown in supporting information, Fig. S1). (c) Variation in total transmission at different wavelengths spanning UV to NIR ranges for each thin film. (d) Schematic of the formation of the TTF through inter-diffusion processes.

During conversion to a TTF, three distinct absorption edges are found in the ITA film and a reduction in total transmission at all wavelengths from 300 nm – 2.5 μm is observed. These additional absorption edges will be shown to be attributed to the initial formation stages of the TTF due to diffusion at the glass-VO interface coupled with the crystallisation of the VO thin film at the VO-Air interface, and characteristic of the initial stages of conversion to the ternary metal oxide. After the completely transparent film is formed, we observe a slight decrease in optical transmission >1100 nm, uniquely after optical clearing. The reduction in transparency is consistent with a reduction in dielectric constant and increase in free carriers at energies less than the plasma frequency (Fig. 1(b), right), where the ITA treated film has a reduced transparency at lower frequencies – observing some opacity in the NIR region for the intermediate films indicates a change in electrical conductivity and film composition, due to the variation in effective refractive index.

The fully transparent HTA treated thin film exhibits just an 8 – 10% reduction in absolute transmission compared to the glass substrate in the 300 – 900 nm range, and a 3 - 5% reduction in the 900 – 2500 nm region, after accounting for the reduced reflectivity from index matching at the TTF-glass interface. From AFM images, the film thickness for this As-Dep thin film, formed from a 10–layer coating of the initial VO film, is ~ 95 - 105 nm (See Supporting Information, Fig. S2 (a)). Diffusion of Na and Si species from the substrate into the thin film results in a phase conversion that promotes optimum transparency of the TTF after annealing at 300 ^{o}C. The UV-Vis spectra show a distinct blue shift in the absorption edge similar to the response of the underlying glass substrate, and broadband transmission is likely limited by the UV absorption in the glass substrate. The final TTF, once fully formed, no longer exhibits any secondary or

tertiary supra band-gap absorption edges as found in the As-Dep and intermediate ITA treated films (Fig. 1(b)).

An effective optical bandgap (E_g) related to each of the absorption edges observed during the conversion from As-Dep to TTF film was estimated using the modified Davis-Mott relation.[27, 46]. The refractive index (*n*) of the material was then estimated using the Moss relation where $n_{VO}^4 E_g \sim 95$ eV.[47, 48] The respective E_g and *n* values for each of the samples are summarised in Table 1.

As the transparency of the thin films increases, an associated increase of the primary E_g value and a decrease in the respective refractive index values is noted. The As-Dep VO film exhibited two absorption edges that can be correlated with E_g values of 2.6 eV and 3.54 eV respectively, while the ITA treated sample displayed three absorption edges at 2.22 eV, 2.74 eV and 3.62 eV. The HTA treated sample has a calculated E_g of 3.7 eV while the glass substrates absorption edge is calculated to be ~4.01 eV. The TTF formation thus mimics the optical transmission of the glass substrate with a consistent high transparency down to 300 nm. The interfacial region thus show index matching with absorption edges close to the substrate. Both the secondary E_g value found in the As-Dep film and the tertiary E_g value seen in the ITA treated films can be attributed to the amorphous and crystalline V_2O_5 thin films deposited using the same technique on an ITO substrate.[27] The secondary absorption edge found for the ITA samples is due to the presence of a region between the layer formed at the glass-VO and VO-Air interfaces, illustrated in Fig. 1(d). The *n* values for each of the primary, secondary and tertiary E_g values were calculated and presented in Table 1. The absorption edges can be attributed to different layers (*vide infra*) formed within the thin film due to both crystallisation and diffusion-based changes in composition.

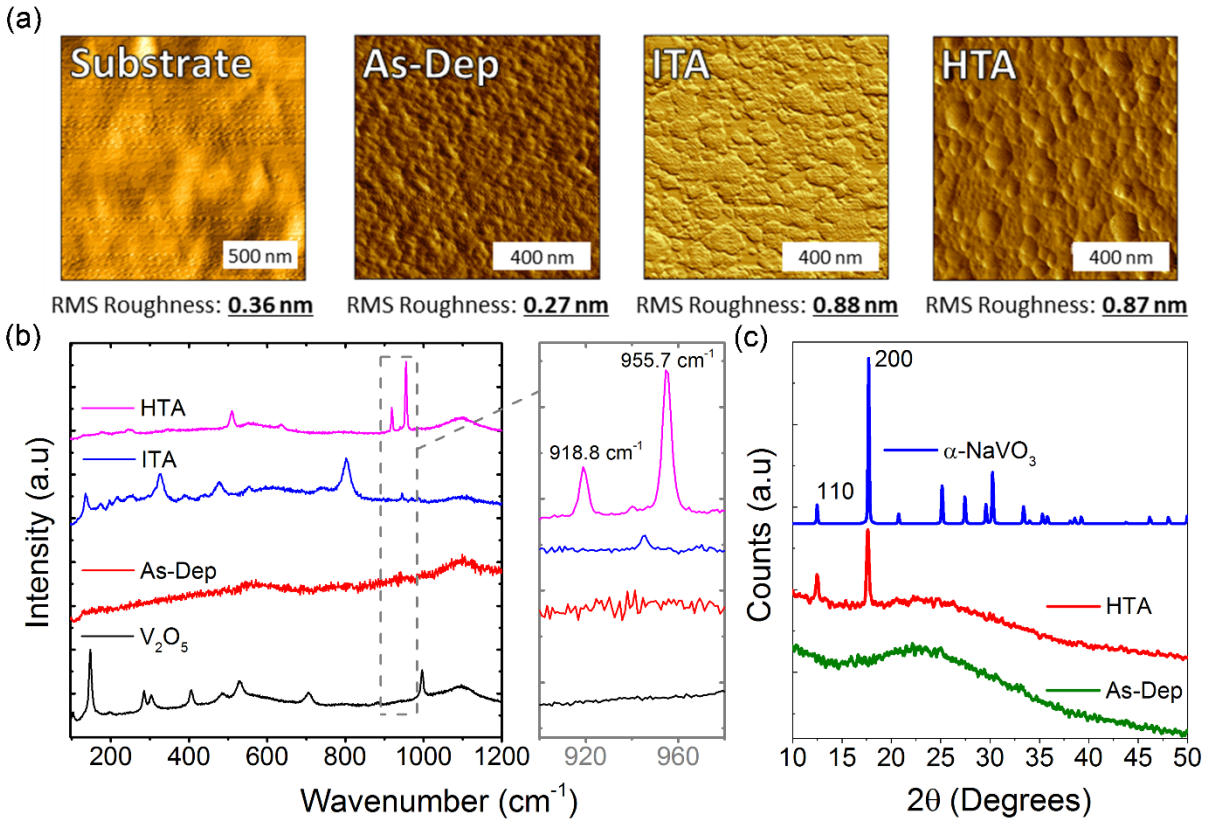

Figure 2. (a) AFM images and respective RMS roughness values for the substrate, As-Dep, ITA and HTA treated thin films. (b) Raman scattering spectroscopy of orthorhombic V_2O_5 on a diffusion layer substrate and As-Dep, ITA and HTA treated thin films on glass substrates showing the formation of the transparent TTF phase. (c) Thin film XRD pattern of As-Dep and HTA thin film confirms the presence of a crystalline metamunirite α-$NaVO_3$ component in the TTF material.

The surface morphology of the thin films was examined using AFM and are presented in Fig. 2 (a), and additional AFM images can be seen in the supporting information Fig. S3. The AFM analysis shows small changes to the surface morphology and grain density during thermal treatment, including a slight increase in surface roughness. During conversion, the ITA films show a granular morphology with inter-grain voids that eventually merge to a fused-grain structure when completely transparent. The average rms surface roughness measured for the As-Dep, ITA and HTA treated films is <1 nm. As seen in both the optical images in Fig. 1 (a) and in

the corresponding AFM images in Fig. 2 (a), the surface of the TTF remains relatively continuous and consistent over the entire sample area.

Using Raman scattering spectroscopy, the vibrational bonds of the As-Dep, ITA and HTA treated films were analysed and compared to that of orthorhombic V_2O_5 in Fig. 2 (b). The As-Dep thin films are composed of amorphous stoichiometric V_2O_5 and show no discernible vibrational bonds – V_2O_5 never crystallizes in the presence of the dopant interacting species. When a transparent diffusion barrier such as ITO or FTO is present between the As-Dep film and the glass substrate, the formation of orthorhombic V_2O_5 occurs, which has an intense and well-defined Raman scattering spectrum.[45, 49, 50] The characteristic diffusion process has been shown to occur at very high thermal treatment temperatures in VO and tungsten oxide (WO_3) thin films where the diffusion initiates from the glass substrate, through an ITO coating layer to form islands of the material[51, 52]. In such a case, the resulting surface film is non-homogeneous and discontinuous allowing species diffusion through voids or gain boundaries.[51, 52] The lack of a diffusion barrier layer on the substrate facilitates diffusion to form a continuous TTF material on the surface of the glass.

The TTF material formed in this study has distinct Raman scattering modes at 509.7 cm^{-1}, 918.8 cm^{-1} and 955.7 cm^{-1}. The TTF vibrational modes are attributed to specific O bonds between the Si, Na and V formed through the diffusion process. Some of the prominent Raman modes are attributed to the formation of a crystalline α-$NaVO_3$ component within the TTF thin film.[53, 54] Many of the Raman scattering modes for the ITA treated films matches superimposed amalgamated spectra for each of the intermediate layers. The thin film XRD patterns in Fig. 2 (c) confirm the formation of crystalline α-$NaVO_3$ within the TTF thin film where diffraction from the α-$NaVO_3$ (110) and (200) planes is present.[55] The (110) and (200) planes in α-$NaVO_3$ are also present in β-$NaVO_3$ indexed to (020) and (110) respectively.[56] The presence of only two

diffraction peaks for the TTF, both of which are common to α-$NaVO_3$ and β-$NaVO_3$, limits definitive prediction of the crystalline phase through XRD alone. However, the Raman scattering spectra are consistent with predominantly α-$NaVO_3$, allowing the crystalline component to be indexed to α-$NaVO_3$. The amorphous background of the As-Dep and HTA XRD patterns located below 40^o implies that the crystalline α-$NaVO_3$ material is surrounded by a non-crystalline glassy matrix.

XPS was used to examine the composition during annealing, which leads to the formation of the TTF. The XPS spectra of the Si 2p, V $2p_{3/2}$ and Na 1s peaks for the substrate, As-Dep, ITA and HTA treated films are shown in Fig. 3 (a). Survey scans were recorded with the adventitious C 1s photoemission at 284.3 eV as a reference (the reference shifts are consistent when using C 1s or O 1s as we observe no scattering of binding energy (BE) values from measurement). A decrease in the BE of ~1.6 eV and ~0.8 eV is measured between the Si 2p and Na 1s core-level photoelectrons of the glass substrate compared to the fully formed TTF. The same associated decrease is found in Na_2O-SiO_2 glasses where an increased amount of Na_2O present in the glass results in a reduced BE of both the Si 2p and Na 1s peaks.[57] In the case of the TTF, the reduction in the Si 2p and Na 1s BE is attributed to the presence of the vanadia species. A small shift in energy of ~0.5 eV is observed for the V $2p_{3/2}$ peak after conversion from the As-Dep to the TTF. This small BE shift is attributed to the conversion of the stoichiometric As-Dep VO thin film to a TTF formed of a crystalline α-$NaVO_3$ within an overall glassy matrix approximating $V_{0.0352}O_{0.547}Si_{0.4078}Na_{0.01}$.

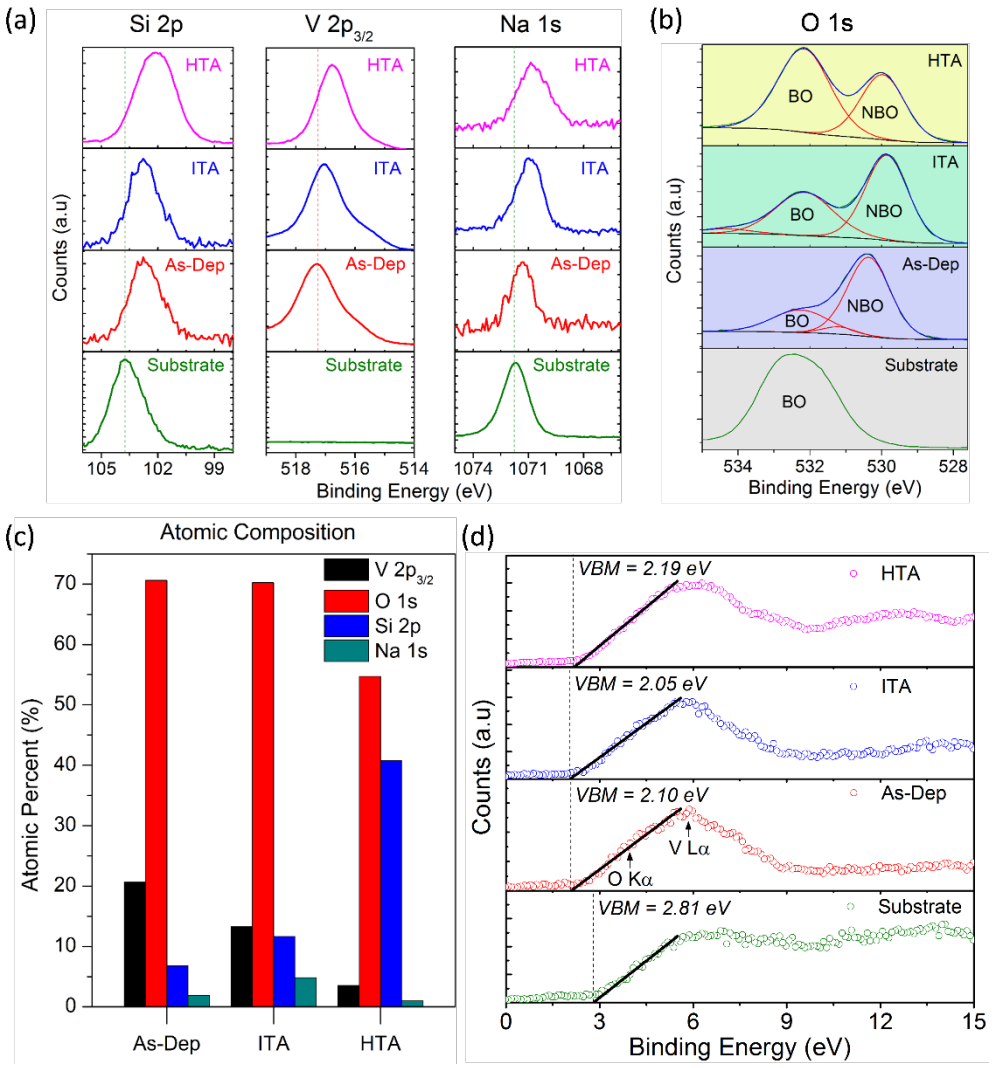

Figure 3. (a) XPS analysis showing the changes in the Si, V and Na spectra during thermal treatment and subsequent diffusion between the substrate and the VO thin film. (b) XPS spectra of the O 1s peaks showing the BO and NBO contributions of the glass substrate, As-Dep, ITA and HTA samples. (c) Relative atomic composition of the surface of the thin films from XPS data during conversion to the $V_{0.0352}O_{0.547}Si_{0.4078}Na_{0.01}$ TTF. (d) Valence band (VB) spectra and VBM estimates for the glass substrate, As-Dep, ITA and HTA treated films.

The glass substrate shows a single contribution to the O 1s peak in Fig. 3 (b) while the As-Dep, ITA and HTA treated films contain two O 1s contributions arising from variations in the bridging of the O atoms to the other species within the thin film.[57] The O 1s peak at a higher BE is assigned to bridging oxygen (BO) atoms while the lower BE peak is due to non-bridging oxygen (NBO) atoms. In a BO system, two Si atoms are bonded by an O (Si-O-Si) while in an NBO system the Si, Na and V atoms can be O bonded in a number of ways (Si-O-V/Na, V=O,

Na-O-V).[58] The ratio between the NBO and total O (TO) peak areas is presented in Table 1 and highlights the dominant type of O bonding within each film. During TTF formation (ITA and HTA treated samples), the NBO/TO ratio is found to reduce as the quantity of Si species within the thin film increases.

Table 1. Surface roughness, optical and material properties of the glass substrate and the respective thick As-Dep, ITA and HTA treated films. The E_g values for each of the films was calculated for the absorption edges present in the UV-Vis transmission spectra. The *n* values were calculated from the corresponding E_g values.

Samples	**Avg. RMS Roughness (nm)**	**E_g (eV)**	***n***	**NBO / TO**	**ΔE_{BO-NBO} (eV)**
Glass	0.36	4.01	1.5171*	n/a	n/a
As-Dep	0.27	3.54, 2.60	2.28, 2.46	0.686	1.8
ITA	0.88	3.62, 2.74, 2.22	2.26, 2.43, 2.56	0.506	2.3
HTA	0.87	3.70	2.25	0.181	2.2

*Refractive index provided from Thermo Scientific, n = 1.5171 at λ = 546.07 nm.

The atomic composition of the thin films was studied using XPS and the calculated Si, Na, O and V at. % for the As-Dep, ITA and HTA treated samples are shown in Fig. 3 (c). The calculated compositions for each of the films are $V_{0.207}O_{0.762}Si_{0.068}Na_{0.019}$ (As-Dep), $V_{0.133}O_{0.724}Si_{0.116}Na_{0.048}$ (ITA) and $V_{0.0352}O_{0.547}Si_{0.4078}Na_{0.01}$ (TTF), respectively. Note, the small Si and Na concentration (in at%) in the As-Dep stoichiometric V_2O_5 thin film is attributed to photoelectron emission from the glass caused by penetration of the X-rays and photoelectron escape through intergrain boundaries in the thin film that is otherwise thicker than the X-ray penetration depth. Analysis of the O 1s spectrum (*vide ante*) shows the majority of the diffused Si, making up ~40% of the TTF composition, is bonded to O in a BO system while the remaining O bonded Si is NBO bonded with the V and Na. Vanadia and Na species constitute ~ 3.5% and 1% of the TTF composition respectively, the majority of which is assumed to be O bonded in an

NBO system; the bonded O BE shifts towards the VB edge as the TTF forms (see Fig. 3(d)) and the strong hybridization of V 3d–O 2p orbitals characteristic of the defined VB spectrum of V_2O_5 (As-Dep) is lost upon conversion to the TTF. The relative V and Na species in the overall ternary composition agrees very well with theoretical V_2O_5 and Na_2O ratios for α-$NaVO_3$ of 74.6 and 25.4 wt%, respectively.[56]

Valence band spectra were also extracted from XPS data from the substrate, As-Dep, ITA and HTA treated films to determine how phase conversion to the mixed metal oxide TTF via the inter-diffusion affects the effective bandgap and density of states. Figure 3 (d) shows the XPS valence band spectra for the As-Dep, ITA and HTA films and the calculated valence band maximum (VBM) was estimated by extrapolation of the leading edge of the photoemission onset.[59] The borosilicate substrate VBM is ~2.89 eV, less than that of pure SiO_2, ~5 eV[59, 60]. The drop in the VBM is attributed to the other species within the substrate. We observe a decrease in the VBM of the As-Dep and ITA films, while the HTA treated thin film exhibits a VBM of 2.19 eV once the TTF is fully formed. Interestingly, the formation of the TTF results in the reappearance of a secondary peak in the 11 – 14 eV region previously found in the substrate, but not present in the As-Dep film. The reappearance of this mode could be due to the inter-diffusion mechanism and attributed to O 2p (Si 3p, Si 3s) bonding states within the TTF film[60] which reappear in the spectra due to the diffusion of Si and O species to the surface of the thin film.

To establish the effect of annealing duration on TTF formation, a time-dependent experiment was performed over varying annealing temperatures at set periods of time. Five layer As-Dep thin films (~50 - 60 nm, see supporting information Fig. S2 (b)) were prepared and cut into multiple pieces. Annealing was performed at 200 ^oC (LTA), 250 ^oC and 300 ^oC with separate samples removed and characterized each hour. A thinner As-Dep thin film was chosen so that TTF conversion could be mapped over a short period of annealing time. Due to the

thinner As-Dep thin film, the intermediate stage studied previously is bypassed in short time and complete transparency is rapidly developed. Figure 4 (a) shows UV-Vis-NIR transmission spectra of the As-Dep, LTA, ITA and HTA treated samples as a function of annealing time. The corresponding optical images of the samples are included as insets in Fig. 4 (a). The corresponding optical images of the films, including the 48 and 72 h LTA films, are shown in supporting information Fig. S4.

Optical transmission analysis shows that a fully formed TTF occurs after 24 h from both the ITA and HTA treated thin films. The LTA treated films, annealed at a lower temperature of 200 °C, do not form a fully transparent TTF after 24 h due to limited substrate species diffusion and phase change. Optical images of the LTA samples after subsequent heating for 48 and 72 h, see supporting information Fig. S3, appear to show the LTA thin films to be optically transparent, however, corresponding UV-Vis-NIR transmission data in Fig. 4 proves that the transparency in the NIR region is reduced compared to ITA and HTA films owing to remnant electro-optic conductivity from limited phase conversion from V_2O_5-based As-Dep film to the ternary oxide TTF.

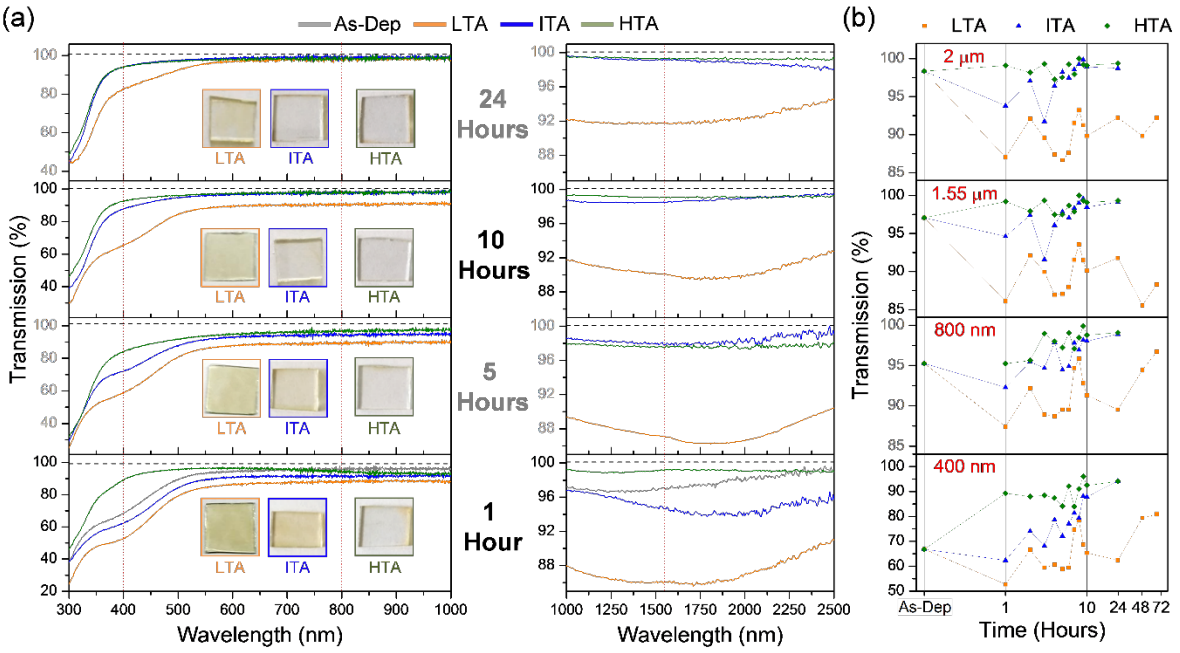

Figure 4. (a) UV-Vis-NIR transmission spectra and optical images of the LTA, ITA and HTA treated samples over time and (b) corresponding percentage transmission at λ = 400 nm, 800 nm, 1.55 µm and 2 µm.

The time-dependent transmission for the As-Dep, LTA, ITA and HTA treated films was measured at 400 nm, 800 nm, 1.55 µm and 2 µm and compared in Fig. 4 (b). The annealing interval at the intermediate stage, which decreases absolute transmission due to densification of the crystalline grains prior to phase conversion to the ternary TTF, is shorter in the 5 layer as-deposited thin film. The thinner as-deposited thin film requires less time ($\sim t^{1/2}$) due to a shorter diffusion length (assuming an invariant ionic diffusion coefficient in the converting phase) to form the TTF. The formation of the TTF from dip-coated films at lower annealing temperatures is beneficial for incorporation into devices that cannot withstand high temperature processing conditions and for optical coatings on curved or bespoke shaped glass and glassy encapsulants, such as the glass tube in Fig. 1 (a). The E_g values for each of the films over time is shown in Fig. 5 (a). Two absorption edges are present in spectra for LTA and ITA treated films. The secondary absorption edge value is attributed to the remnants of the intermediate stage within the thin film,

which disappear in the late stage of the annealing in ITA films when modified to complete transparency. The primary E_g value of ~3.6 eV of the TTF forms in both the ITA and HTA films after 24 h annealing while in the LTA films a primary E_g value higher than 3.6 eV at the time points prior to 24 h. The higher LTA primary absorption E_g value is attributed to a contribution from the underlying glass substrate and the ITA film which due to a lower temperature does not form the TTF through diffusion processes until a late stage in the annealing; therefore the glass substrate with a higher absorption edge influences the absorption edge of the ITA films.

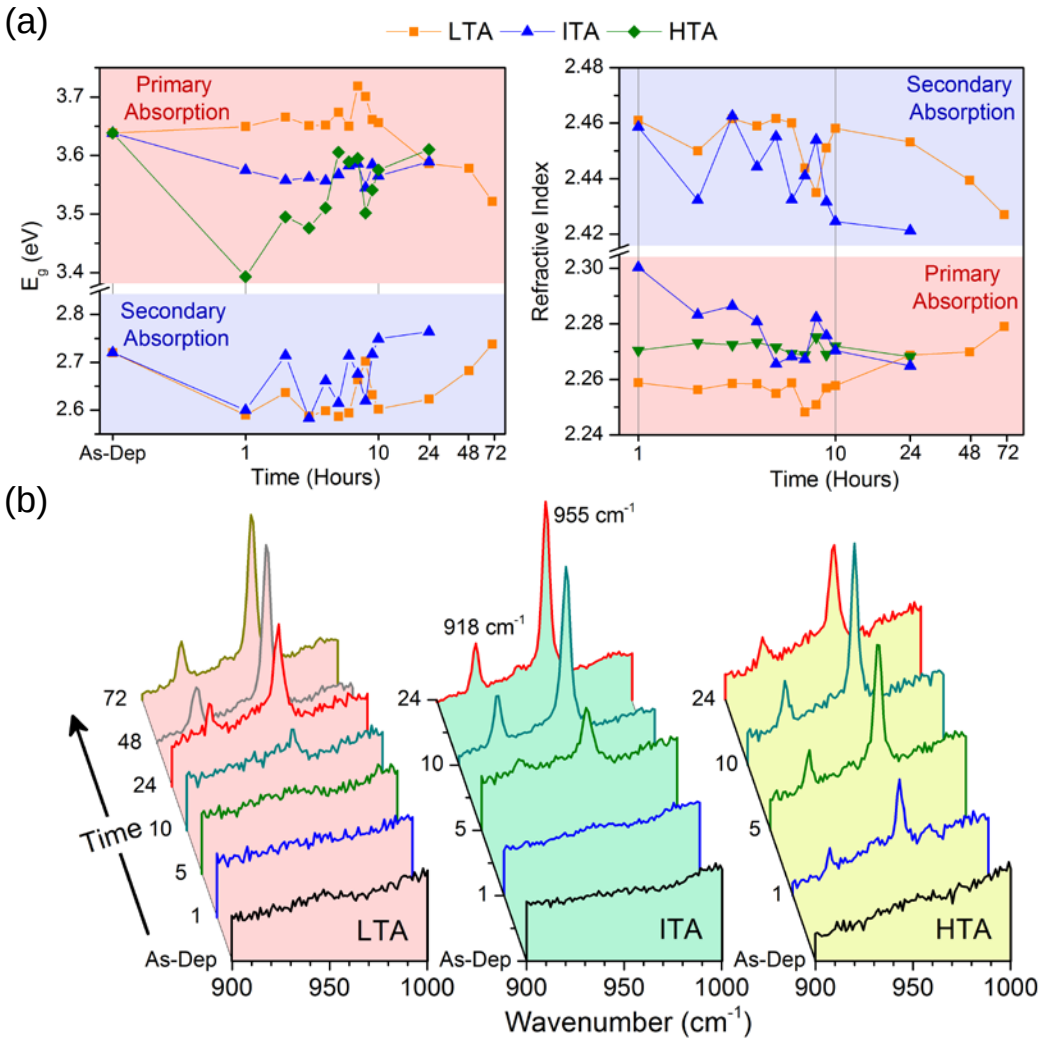

Figure 5. (a) Calculated E_g and n values for the primary and secondary absorption edges of the LTA, ITA and HTA treated films, respectively. (b) Time-dependent Raman scattering spectra of LTA, ITA and HTA treated samples showing the formation of the 918 cm^{-1} and 955 cm^{-1} vibrational peaks at each of the thermal treatment temperatures.

By comparison of refractive index data in Fig. 5(a) and transmission characteristics in Fig. 4(b), we find that the enhanced transmission from optical clearing of the film to a TTF occurs because of a phase change to a ternary mixed metal oxide that widens the transmission window and overall transparency, and from reduced interfacial reflectivity with the glass substrate.

Raman scattering spectroscopy shown in Fig. 5 (b) was used to map the phase conversion via diffusion during TTF formation, by monitoring the onset of the two characteristic vibrational peaks at 918.8 cm^{-1} and 955.7 cm^{-1} respectively over time for the LTA, ITA and HTA films. The full time-dependent Raman scattering spectra can be found in the supporting information Fig. S5. The characteristic vibrational peaks indicative of crystallized phase conversion to the ternary mixed oxide TTF appear after only 1 h of annealing at 300 ^{o}C (HTA), after 4 h under annealing at 250 ^{o}C (ITA), and begins to appear after 10 h when heated at 200 ^{o}C (LTA). The intensity and resolution of the 918.8 cm^{-1} and 955.7 cm^{-1} vibrational peaks also markedly increases in each case with time once the TTF begins to form, until all films are transparent. While the absolute transmission of the LTA films never matches that of the ITA and HTA treated films, the LTA treated samples do show the formation of the same characteristic Raman vibrational peaks. The formation of the characteristic Raman modes within the LTA samples confirm that the onset of TTF formation via inter-diffusion occurs at 200 ^{o}C. Species diffusion was considered be assuming random lattice diffusion of Si, O, Na species into the initially amorphous V_2O_5 film with net radial displacement of atomic or ionic diffusion unidirectionally from the substrate (into or indeed out of) the ~50 nm thick 5-layer dip-coated layer. The thermal diffusivity of the glass (~0.35 mm/s) ensures fast equilibration to the annealing temperature, leaving the temporal phase conversion process specifically a function of ionic diffusivity and atomic restructuring. Using the

Si as the tracer (7% to 40% concentration increase upon TTF formation, *cf.* Fig. 3(c)), we estimate an average diffusion constant of just $D = 3.5 \times 10^{-15}$ cm^2 s^{-1} (for Na in sodium silicate glasses, $D = 10^{-10}$-10^{-11} cm^2 s^{-1}), and thus the diffusion of species into the film is the faster process; subsequent diffusion within the developing TTF is slower, and confirmed from Raman scattering evidence of the onset of TTF formation (but prior to diffusion and subsequent complete chemical modification) and via XPS at% noted during the TTF formation.

The UV-Vis-NIR transmission characteristics of the samples indicates that to form the fully transparent TTF material, the extra thermal energy experienced by the ITA and HTA treated samples over longer time periods is required to fully convert the entire film (*cf.* Fig. 1(d) and develop full broadband transparency.

4 Conclusions

A UV-Vis-NIR broadband ternary V-O-Na-Si mixed metal oxide transparent thin film material was demonstrated to form on glass through a diffusion controlled process from a solution processed dip-coated VO thin film. The method itself is a facile and cost-effective technique for the production of a transparent layer on the borosilicate glass surface that is conformal and generally free of cracks or pinholes. The final TTF material retains a low surface rms roughness of <1 nm and a defined composition and structure from the embedding and mixing of the V-O and Na-O and Si-O species. XPS, Raman scattering and XRD analysis confirm a TTF surface composition of $V_{0.0352}O_{0.547}Si_{0.4078}Na_{0.01}$, that contains a crystalline α-$NaVO_3$ component within a glassy matrix. The transparency of the TTF exceeds 90-97% absolute transmission across the UV to NIR wavelength range. The nature of O bonding within this transparent material modifies

during annealing from a higher proportion of NBO in the As-Dep V_2O_5 to a dominant BO configuration with Si-O and Na during the formation of the TTF.

During the annealing to form the TTF, an intermediate stage forms a multi layered system, with each layer exhibiting unique optical and structural characteristics analogous to a multi layered oxide system with a lower absolute transparency to both the as-deposited and TTF materials. The TTF formation was demonstrated to be possible at lower temperatures using initially thinner dip-coating, and provides a faster, thinner TTF optical coating on glass in shorter time, which is of benefit for incorporation into optoelectronic devices, (tandem) solar cells, LEDs and for optical coatings where enhanced and defined transmission/reflection characteristics are needed, but where high annealing temperatures must be avoided, all below softening temperatures for a range of glasses, optics and encapsulants. The approach may also allow low- or high-k binary, ternary or other dielectric oxide growth, and as an anti-tarnish barrier layer invisible to the human eye.

The adaptable processing techniques involved in the formation of a V-O-Na-Si based TTF material on glass substrates via precursor design and high rate dip-coating is practical for technologies in optics and photonics. Importantly, TTFT and optical coatings research and development for next generation display and interactive technologies require new materials with higher electronic mobilities, controllable thickness and refractive index, application-specific absorbance characteristics facilitates by doping using alternative metals than those reported here, and ease in processability. The latter is particularly important for devices or optics with complex or non-planar shapes. With the advent of flexible and shape-adaptable displays and screens, the use of plastic substrates is also increasing in importance owing to their light weight, flexibility, and low cost and the use of the substrate composition is an intriguing method to dope, control and compositionally modify optical coatings. Indeed, this approach opens the door to using not

only substrates, but coatings on substrates as metal or dopant sources for thermally driven diffusional modification of subsequent optical or optoelectronic coating materials.

5 Acknowledgments

C.G. acknowledges the support of the Irish Research Council under award RS/2011/797. We acknowledge support from the Irish Research Council Ulysses Scheme and from a New Foundations Award. This work was also supported by Science Foundation Ireland (SFI) under the National Access Programme (NAP 417), and through an SFI Technology Innovation and Development Award under contract no. 13/TIDA/E2761.

6 References

1. K. Ellmer, *Nat. Photon*, 2012, **6**, 809-817.
2. E. Fortunato, P. Barquinha and R. Martins, *Adv. Mater.*, 2012, **24**, 2945-2986.
3. C. G. Granqvist, *Thin Solid Films*, 2014, **564**, 1-38.
4. C.-P. Chen, Y.-D. Chen and S.-C. Chuang, *Adv. Mater.*, 2011, **23**, 3859-3863.
5. X.-L. Zhang, J.-F. Song, X.-B. Li, J. Feng and H.-B. Sun, *Appl. Phys. Lett.*, 2013, **102**, 103901.
6. Y. Wang, L. Liu, L. Xu, X. Cao, X. Li, Y. Huang, C. Meng, Z. Wang and W. Zhu, *Nanoscale*, 2014, **6**, 6790-6797.
7. H. Dotan, O. Kfir, E. Sharlin, O. Blank, M. Gross, I. Dumchin, G. Ankonina and A. Rothschild, *Nat. Mater.*, 2013, **12**, 158-164.
8. R. M. Pasquarelli, D. S. Ginley and R. O'Hayre, *Chem. Soc. Rev.*, 2011, **40**, 5406-5441.
9. M. Faustini, L. Nicole, C. Boissière, P. Innocenzi, C. Sanchez and D. Grosso, *Chem. Mater.*, 2010, **22**, 4406-4413.
10. D. Chen, *Sol. Energy Mater. Sol. Cells*, 2001, **68**, 313-336.
11. M. A. Kats, S. J. Byrnes, R. Blanchard, M. Kolle, P. Genevet, J. Aizenberg and F. Capasso, *Appl. Phys. Lett.*, 2013, **103**, 101104.
12. J. Jang, R. Kitsomboonloha, S. L. Swisher, E. S. Park, H. Kang and V. Subramanian, *Adv. Mater.*, 2013, **25**, 1042-1047.
13. K. Si Joon, Y. Seokhyun and K. Hyun Jae, *Jpn. J. Appl. Phys.*, 2014, **53**, 02BA02.
14. Y.-H. Lin, H. Faber, J. G. Labram, E. Stratakis, L. Sygellou, E. Kymakis, N. A. Hastas, R. Li, K. Zhao, A. Amassian, N. D. Treat, M. McLachlan and T. D. Anthopoulos, *Adv. Sci.*, 2015, **2**.
15. A. Grill, S. M. Gates, T. E. Ryan, S. V. Nguyen and D. Priyadarshini, *Appl. Phys. Rev.*, 2014, **1**, 011306.

16. W.-J. Lee, W.-T. Park, S. Park, S. Sung, Y.-Y. Noh and M.-H. Yoon, *Adv. Mater.*, 2015, **27**, 5043-5048.
17. K. L. Choy, *Prog. Mater Sci.*, 2003, **48**, 57-170.
18. G. H. Jeon, *J. Phys. D: Appl. Phys.*, 2009, **42**, 043001.
19. T. Schneller, R. Waser, M. Kosec and D. Payne, *Chemical Solution Deposition of Functional Oxide Thin Films*, Springer, London, 1st edn., 2013.
20. J.-W. Jo, J. Kim, K.-T. Kim, J.-G. Kang, M.-G. Kim, K.-H. Kim, H. Ko, Y.-H. Kim and S. K. Park, *Adv. Mater.*, 2015, **27**, 1182-1188.
21. X. Bao, Q. Zhu, T. Wang, J. Guo, C. Yang, D. Yu, N. Wang, W. Chen and R. Yang, *ACS Appl. Mater. Interfaces*, 2015, **7**, 7613-7618.
22. K. K. Banger, Y. Yamashita, K. Mori, R. L. Peterson, T. Leedham, J. Rickard and H. Sirringhaus, *Nat. Mater.*, 2011, **10**, 45-50.
23. J. H. Chang, K. M. Chiang, H. W. Kang, W. J. Chi, J. H. Chang, C. I. Wu and H. W. Lin, *Nanoscale*, 2015, **7**, 4572-4579.
24. Z. Chen, W. Li, R. Li, Y. Zhang, G. Xu and H. Cheng, *Langmuir*, 2013, **29**, 13836-13842.
25. N. Mizoshita, M. Ishii, N. Kato and H. Tanaka, *ACS Appl. Mater. Interfaces*, 2015, **7**, 19424-19430.
26. M. Faustini, B. Louis, P. A. Albouy, M. Kuemmel and D. Grosso, *J. Phys. Chem. C*, 2010, **114**, 7637-7645.
27. C. Glynn, D. Creedon, H. Geaney, E. Armstrong, T. Collins, M. A. Morris and C. O'Dwyer, *Sci. Rep.*, 2015, **5**, 11574.
28. H. Minemawari, T. Yamada, H. Matsui, J. y. Tsutsumi, S. Haas, R. Chiba, R. Kumai and T. Hasegawa, *Nature*, 2011, **475**, 364-367.
29. S. T. Meyers, J. T. Anderson, C. M. Hung, J. Thompson, J. F. Wager and D. A. Keszler, *J. Am. Chem. Soc.*, 2008, **130**, 17603-17609.
30. D. Grosso, *J. Mater. Chem.*, 2011, **21**, 17033-17038.
31. S. R. Thomas, P. Pattanasattayavong and T. D. Anthopoulos, *Chem. Soc. Rev.*, 2013, **42**, 6910-6923.
32. T. O. L. Sunde, E. Garskaite, B. Otter, H. E. Fossheim, R. Saeterli, R. Holmestad, M.-A. Einarsrud and T. Grande, *J. Mater. Chem.*, 2012, **22**, 15740-15749.
33. C. O'Dwyer, M. Szachowicz, G. Visimberga, V. Lavayen, S. B. Newcomb and C. M. S. Torres, *Nat. Nanotechnol.*, 2009, **4**, 239-244.
34. J.-Y. Lee, S. T. Connor, Y. Cui and P. Peumans, *Nano Lett.*, 2008, **8**, 689-692.
35. S. Watcharotone, D. A. Dikin, S. Stankovich, R. Piner, I. Jung, G. H. B. Dommett, G. Evmenenko, S.-E. Wu, S.-F. Chen, C.-P. Liu, S. T. Nguyen and R. S. Ruoff, *Nano Lett.*, 2007, **7**, 1888-1892.
36. C. O'Dwyer and C. Sotomayor Torres, *Front. Phys.*, 2013, **1**.
37. R. A. Street, *Adv. Mater.*, 2009, **21**, 2007-2022.
38. K. Nomura, H. Ohta, A. Takagi, T. Kamiya, M. Hirano and H. Hosono, *Nature*, 2004, **432**, 488-492.
39. H. Q. Chiang, J. F. Wager, R. L. Hoffman, J. Jeong and D. A. Keszler, *Appl. Phys. Lett.*, 2005, **86**, 013503.
40. Y. Ya-Hui, S. S. Yang, K. Chen-Yen and C. Kan-San, *Electron Devic. Lett. IEEE*, 2010, **31**, 329-331.
41. C. Piccirillo, R. Binions and I. P. Parkin, *Chem. Vap. Deposition*, 2007, **13**, 145-151.
42. T. Paik, S. H. Hong, E. A. Gaulding, H. Caglayan, T. R. Gordon, N. Engheta, C. R. Kagan and C. B. Murray, *ACS Nano*, 2014, **8**, 797-806.

43. Z. Yang, C. Ko and S. Ramanathan, *Annu. Rev. Mater. Res.*, 2011, **41**, 337-367.
44. Z. Tong, J. Hao, K. Zhang, J. Zhao, B.-L. Su and Y. Li, *J. Mater. Chem. C*, 2014, **2**, 3651-3658.
45. C. Glynn, D. Aureau, S. O'Hanlon, L. Daly, H. Geaney, G. Collins, A. Etcheberry and C. O'Dwyer, *ECS Trans.*, 2015, **64**, 1-9.
46. J. Tauc, *The Optical Properties of Solids*, Academic Press, New York, 1966.
47. Y. Akaltun, M. A. Yıldırım, A. Ateş and M. Yıldırım, *Opt. Commun.*, 2011, **284**, 2307-2311.
48. N. M. Ravindra, P. Ganapathy and J. Choi, *Infrared Phys. Techn.*, 2007, **50**, 21-29.
49. C. Glynn, D. Creedon, H. Geaney, J. O'Connell, J. D. Holmes and C. O'Dwyer, *ACS Appl. Mater. Interfaces*, 2014, **6**, 2031-2038.
50. S. O'Hanlon, C. Glynn and C. O'Dwyer, *ECS J. Solid State Sci. Technol.*, 2015, **5**, R3100-R3106.
51. M. Castriota, N. Epervrier, T. Barone, G. De Santo and E. Cazzanelli, *Ionics*, 2007, **13**, 205-211.
52. M. Castriota, T. Caruso, A. Policicchio, S. La Rosa, R. G. Agostino and E. Cazzanelli, *Chem. Phys. Lett.*, 2009, **478**, 195-199.
53. D. de Waal, *Mater. Res. Bull.*, 1991, **26**, 893-900.
54. S. Seetharaman, H. L. Bhat and P. S. Narayanan, *J. Raman Spectrosc.*, 1983, **14**, 401-405.
55. M. Morris, H. F. McMurdie, E. H. Evans, B. Paretzkin, H. S. Parker, N. C. Panagiotopoulos and C. R. Hubbard, *Nat. Bur. Stand.*, 1981, **25**, 67.
56. H. Evans, *Mineral. Mag.*, 1991, **55**, 509-513.
57. H. W. Nesbitt, G. M. Bancroft, G. S. Henderson, R. Ho, K. N. Dalby, Y. Huang and Z. Yan, *J. Non-Cryst. Solids*, 2011, **357**, 170-180.
58. A. Mekki, G. D. Khattak, D. Holland, M. Chinkhota and L. E. Wenger, *J. Non-Cryst. Solids*, 2003, **318**, 193-201.
59. S. W. King, J. Brockman, M. French, M. Jaehnig, M. Kuhn and B. French, *J. Appl. Phys.*, 2014, **116**, 113703.
60. F. G. Bell and L. Ley, *Phys. Rev. B*, 1988, **37**, 8383-8393.